LARGE EDDY SIMULATION OF THE TURBULENT FLOW IN HEATED CURVED DUCTS : INFLUENCE OF THE REYNOLDS NUMBER

Cécile Münch
L.E.G.I Institut de Mécanique de Grenoble,
B.P. 53, 38041 Grenoble Cedex 09, FRANCE
cecile.munch@hmg.inpg.fr

Olivier Métais
Olivier.Metais@hmg.inpg.fr

ABSTRACT

Large-Eddy Simulations (LES) of the turbulent compressible flow within heated curved ducts of square cross section are presented. The aim here is to predict the three-dimensional structures which develop inside cooling channels of rocket engines and study their effect on heat transfer rates. In this work, we focus on the influence of the Reynolds number on these structures and thus on the heat transfer characteristics. We first consider non heated curved ducts for two Reynolds numbers : 6000 and 12000. We observe that the the Ekman vortices corresponding to the secondary flow created by the radial pressure gradient become larger in size at high Reynolds number. The Görtler vortices appearing on the concave wall, due to the centrifugal instability, are conversely smaller and more numerous. We then present simulations with heat: a constant heat flux is imposed on the convex wall of the curved duct. The Ekman vortices are found to be associated with an important transverse temperature gradient on the heated wall. This gradient intensifies when the Reynolds number is increased.

INTRODUCTION

The prediction of the heat transfers in ducts with curvature is a great challenge for engineering applications like gas turbine design, heat exchanger or cooling channels for rocket engine. Several experimental investigations have been devoted to centrifugal instabilities. The streamline curvature and the associated pressure gradient generates a strong secondary flow of Prandtl's first kind as described by Chang et al. (1983), Humphrey et al. (1981). Its intensity can reach more than 20 % of the bulk velocity depending on the curvature radius and takes the shape of two large counter rotating coherent structures, called Ekman vortices. The concave curvature generates a centrifugal instability and Görtler vortices develop near this wall (Hunt and Joubert (1979)): further downstream, these are moved toward the convex wall by the radial pressure gradient. The curved walls have opposite effect on the flow : the concave wall tends to destabilize the flow whereas stabilizing effect is created by the convex side, as noticed by Muck et al. (1985) and Hoffman et al. (1985). Numerical studies of this type of flow have been performed by Moser and Moin (1987), Humphrey et al. (1981) and Silva Lopez and Piomelli (2003) : the difficulty is to predict with precision the secondary flow and the related turbulence characteristics. When heat transfer and curved effect are combined, experiments are fewer. Johnson and Launder (1985) investigate heated square-sectioned U-bend and show that the heat transfer is enhanced on the concave wall and reduced on the convex side compared to a flat wall as found by Mayle et. al (1979). Hébrard et al. (2004) and Münch et al. (2004) study the combined effect of curvature and heating in a closed duct for turbulent flow using the same numerical code as in the present study. We here perform Large Eddy Simulation (LES) in a heated curved duct to investigate the influence of the Reynolds number on the flow dynamics and on the heat transfer. In the previous works mentioned above an imposed temperature higher on one curved wall was imposed. To simulate situations in closer correspondence with industrial configurations, we present simulations with a uniform heat flux on the convex wall.

NUMERICAL CONFIGURATION

The computer code used for our calculations solves the LES modified three dimensional compressible Navier Stokes equations in curved square ducts (see Salinas and Metais (2002)). The subgrid-scale model is the selective structure function model proposed by Lesieur and Métais (1996). To close the system of formed by the momentum and energy equations , we use three supplementary relations. The Sutherland empirical law describe the molecular viscosity variation with temperature. The gas is considered as an ideal gas with the corresponding equation of state and the turbulent Prandtl number is equal to 0.6. The system of equations in generalized coordinates is solved by mean of the corrector-predictor McCormack scheme with a compact extension devised by Kennedy and Carpenter (1997). The scheme is of second order in time and fourth order in space. To provide a fully turbulent inlet boundary condition in the curved duct, a LES of a periodic duct, with all its walls at an imposed temperature T_w, is carried out at the same time. This longitudinally straight periodic duct is linked to the spatially growing duct through the characteristics conditions proposed by Poinsot and Lele (1992). At the outflow of the curved duct, we also used these conditions by imposing the pressure. The wall boundary conditions are no-slip. We here consider two different values of the Reynolds number based upon the bulk velocity : $Re = 6000$ and 12000. The Mach number is taken equal to 0.5, and the Prandtl number is equal to 0.7. We use curvilinear coordinates, s in the streamwise direction, n in the direction normal to the curved

wall and z in the spanwise direction. The origin of the n coordinate is taken on the concave wall. The different lengths are normalized by the hydraulic diameter D_h. All simulations are performed in a curved computational domain of size : $13D_h \times D_h \times D_h$, the curved part is characterized by an inner curvature radius of $10D_h$ and an angle of 30 degrees, see figure 1. The origin O is taken at the inflow on the concave side. The computational domain is discretized using non uniform numerical meshes : a medium grid with $160 \times 50 \times 50$ nodes or a finer grid with $183 \times 66 \times 66$ nodes, along s, n and z directions respectively. An hyperbolic-tangent stretching is applied in the transverse directions n and z, so that $n^+ = z^+ = 1.8$ in wall units. Another stretching in the s direction is applied to avoid the creation of spurious reflected waves. We defined mean quantities as the averaging in time

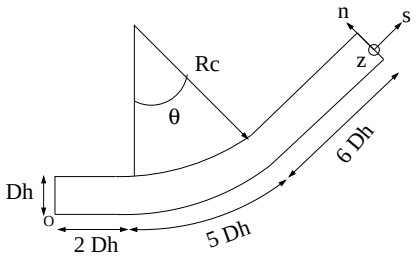

Figure 1: geometry of the duct

: we note $< f(s,n,z) >$ the mean value for any quantity f(s,n,z,t). The mean components of the velocity : $< u >$, $< v >$ and $< w >$ are noted U, V and W, and normalized by the bulk or the local friction velocities. The bulk quantity f_b corresponds with $< f >$ integrated along the two transverse coordinates. The friction velocities $U_{\tau_{cc}}$ and $U_{\tau_{cv}}$ are based on the wall shear stresses τ_{cc} and τ_{cv} respectively on the concave and the convex wall. We called n^+ the distance, from the considered wall, normalized by the local viscous thicknesses. The mean temperature, noted T, is normalized by T_w. We use the fact that the plane $z/D_h = 0.5$ is a symmetry plane for some of the results.

RESULTS

Non heated ducts.

We first carried out simulations without heating : the temperature is the same on each wall of the curved duct and is fixed to a constant value T_w. To validate our grid resolution, we compare simulations performed with the two different grids described above at a Reynolds number equal to 6000. On figure 2, the longitudinal velocity profile U^+ in the symmetry plane non-dimensionalized by the friction velocity $U_{\tau_{cc}}$ is represented in function of the distance to the concave wall n^+.

The displayed log law, defined below, has been proposed by Gavrilakis for flow in square straight duct, taking into account the modification induced by the secondary flow.

$$U^+ = 3.2 \log n^+ + 3.9 \qquad (1)$$

We observe a good fit with the theoretical law near the inlet. The results turn out to be independent of the grid resolution and the medium mesh is sufficient for the simulations at $Re = 6000$. All the results presented below will be based on the

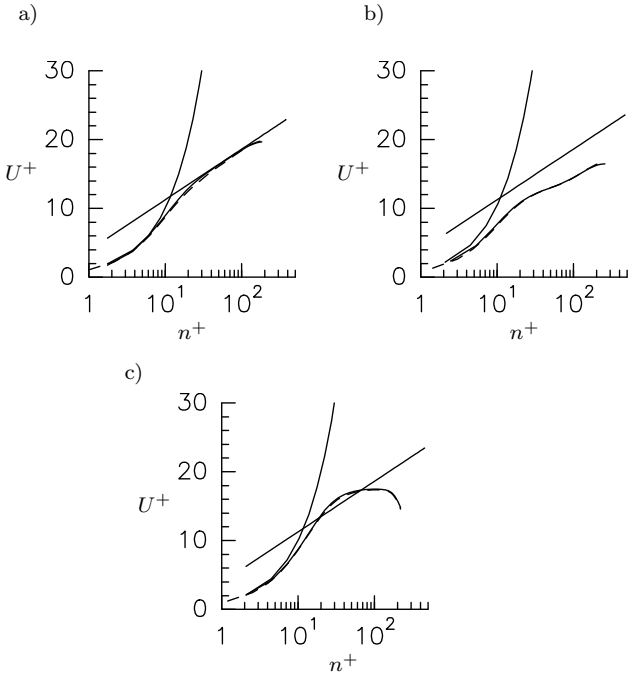

Figure 2: U^+ profile for ——— medium, - - - fine grid a) at the inflow, b) the middle of the curved part, c)the outflow.

medium mesh for the Reynolds number 6000 and on the finer mesh for 12000. This choice of mesh allows to keep the same minimum values for n^+ and Δs^+ (longitudinal direction) in both cases.

In rectilinear ducts of square cross sections, a secondary transverse flow perpendicular to the bulk flow and denominated as Prandtl's second kind, appears near the duct corners. Eight counter rotating vortices, two in each corner, developed. Their intensity is relatively weak : 2% of the bulk velocity. On figure 3, we represent those secondary flows in various cross sections for both simulations at different Reynolds number. On figures 3 a) and b), we first compare the secondary flow at the inflow of the computational domains. We observe that the LES are perfectly able to reproduce this weak secondary flow. We furthermore notice that, when the Reynolds number increases, the secondary vortices are located closer to the duct corner. This result was previously found in the experiments by Gessner (1973). Further downstream of the duct, curvature effects are present and new instabilities appear. The pressure gradient between the concave and the convex wall now gives rise to two intense secondary vortices called Ekman vortices whose intensity is of the order of 20% of the bulk velocity. This intensity is similar for both Reynolds values. These vortices occupy almost the whole width of the duct at the outflow and their center is located in the vicinity of the convex wall (Münch et al. (2004)). When the Reynolds number is equal to 12000, the boundary layers are thinner due to the reduced viscosity. This implies that the recirculating vortices can occupy a larger space within the duct core and their center is moved towards away from the walls as compared with the simulation at Reynolds number 6000 (cf. figures 4 a) and b)).

Close to the concave wall, the lack of balance between the centrifugal forces and the radial pressure gradient gives rise to the well known Görtler vortices. On figure 5, we show iso surfaces of positive Q with $Q = 0.6U_b^2/D_h^2$ and $Q = 0.8U_b^2/D_h^2$ in

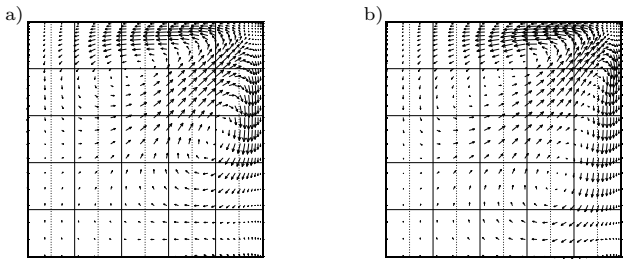

Figure 3: Cross section of the mean secondary flow at the inflow in a quarter of the duct, a) $Re = 6000$, b) $Re = 12000$

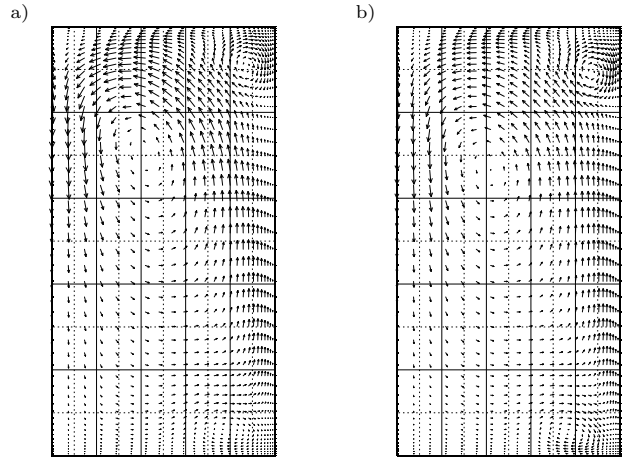

Figure 4: Half cross sections of the mean secondary flow at the outflow : a) $Re = 6000$, b) $Re = 12000$

the curved part for $Re = 6000$ and $Re = 12000$ respectively. This criterion based on Q, second invariant of the velocity derivative tensor (see Hunt et al.(1988)), allows to identify the coherent structures. Görtler vortices appear at the beginning of the curved part and are subsequently moved from the concave toward the convex wall. At Reynolds number equal to 12000, the observed structures are more numerous and smaller in size than in the 6000 case (cf. figure 5): the turbulent structures indeed scale on the viscous length which is smaller when the viscosity is reduced.

We next check the Reynolds number impact on the velocity profiles. On the left of figure 6, the local friction velocity U_τ calculated on each curved wall (concave and convex) is plotted in the duct symmetry plane. The two vertical lines on the left part of figure 6 respectively represent the beginning and the end of the curved part. The formation of the two Ekman vortices strongly influences the friction velocity on both walls: on the concave wall, the friction velocity continuously increases in the curved part due to the reinforcement of the Ekman vortices which generate an impinging flow on the concave wall. Conversely, on the convex wall, the friction velocity decreases since the Ekman vortices yields a flow away from the convex wall. The behavior is similar for both Reynolds number values. We check that the friction velocity decreases when the Reynolds increases.

We now show, on figure 7, the profile of $U^+ = \frac{U}{U_{\tau_i}}$ in the symmetry plane close to each curved wall ($i = cc$ or cv) at the

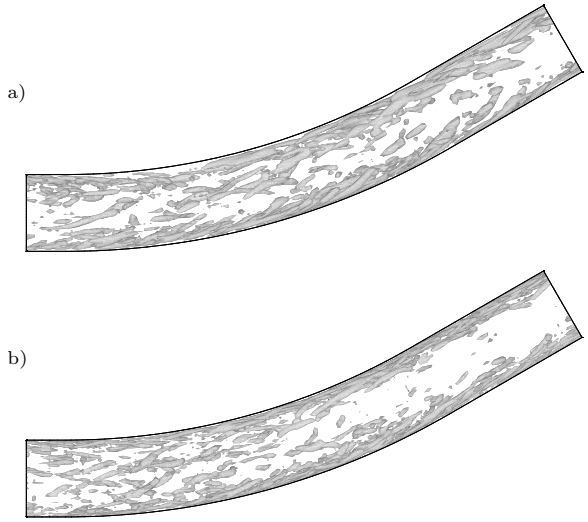

Figure 5: Iso surfaces of Q criterion in the curved part : a) $Re = 6000$, b) $Re = 12000$

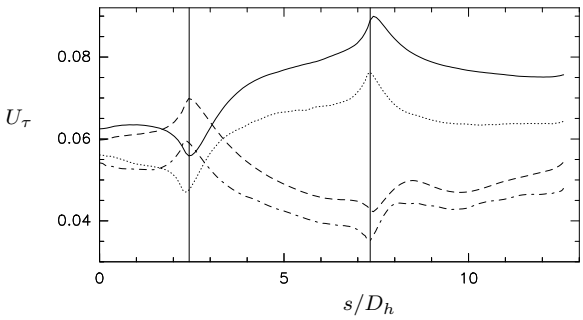

Figure 6: Profiles of U_τ for $Re = 6000$ ——— and - - - and for $Re = 12000$ ····· and —·— on the concave and the convex wall respectively

inflow, in the middle of the curved part and at the outflow. U^+ is plotted in function of the distance the curved wall considered. At the duct inlet, we observe that the profile of U^+ is almost similar for the two Reynolds numbers. The modification of the secondary flow induces a slight velocity increase for the higher Reynolds number case in the logarithmic zone. As shown on figure 3, the counter rotating vortices develop closer to the corner, their influences on the velocity profile are weaker. In the middle of the curved part, U^+ is higher than the theoretical logarithmic law close to the convex wall and lower close to the concave wall. This is due to the fact that the longitudinal pressure gradient is favorable on the convex wall and adverse on the opposite wall. The two U^+ profiles are still very close for both Reynolds numbers. At the outflow, the Reynolds number has a significant effect on the flow behaviour due to the significant modification on the secondary flow showed on figure 4.

Heated ducts

In this part, we investigate the influence of the Reynolds number on heat transfer. For the considered Reynolds num-

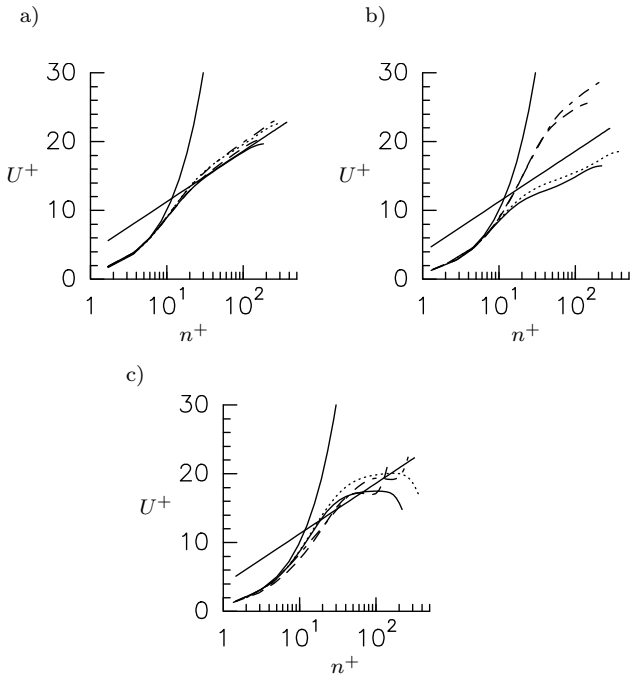

Figure 7: Profiles of U^+ for $Re = 6000$ ——— and - - - and for $Re = 12000$ ····· and —·— on the concave and the convex wall respectively : a) at the inflow, b) the middle of the curved part, c)the outflow.

bers, the gravitational effects are found to be negligible and all the observed flow modifications are imputable to compressibility. On the convex wall of the curved duct, a constant heat flux, H_w, is applied. H_w, defined below, is associated with a Nusselt number taken equal to 6 ($k(T)$ is the fluid conductivity).

$$H_w = k(T)\frac{\partial T(s,n,z)}{\partial n}|_{\frac{n}{D_h}=1} \tag{2}$$

$$Nu = H_w/(k(T_w)T_w/D_h) \tag{3}$$

Two simulations with heating are carried with the two values of Reynolds number 6000 and 12000: the grid resolutions are identical to the non heated case.

The spatial development of the thermal boundary layer is first shown on figure 8 through the instantaneous temperature in the symmetry plane of the curved duct for each value of the Reynolds number. In both cases, the thermal boundary layer thickness reaches $n/D_h \approx 0.5$ at the outflow. It can be observed, that the fluctuations of the temperature are more important when the Reynolds increases. From the beginning of the curved part, ejections of hot fluid take place on the hot wall. We observe that the increase in the Reynolds number induces an augmentation in the size of the turbulent ejections of hot fluid and the latter are more frequent along the duct at the higher Reynolds.

On figure 9, the mean secondary flow and the mean temperature isolines are represented in a cross section at the end of the curved part. The outer line for the temperature corresponds to $T/T_w = 1.1$. The secondary flow plays a major role in the heat transfer. Close to the sidewalls, high speed cold fluid first impacts the heated wall and then converges towards the duct symmetry plane: in this convergence phase it

Figure 8: Instantaneous temperature in the symmetry plane for a) $Re = 6000$ and b) $Re = 12000$, darker color corresponds to higher temperature.

is heated by the heated wall. The central convergence region near the heated wall therefore constitutes a stagnation region where the temperature reaches its maximum. The hot fluid is subsequently ejected from this region towards the duct core.

Figure 10 displays the same quantities as figure 9 but in a cross-section at the end of the duct. The intensity of the secondary flow is weaker than in the curved part, but the two recirculation cells are closer to each other. The pocket of hot fluid is larger in size, compared with figure 9, and we observe that the hot fluid reaches $n/D_h \approx 0.4$ in the symmetry plane for both Reynolds values. Since the Ekman cells are wider at $Re = 12000$, as showed in the first part, the thermal boundary layer thickness is larger for the higher Reynolds number case (figure 10 b)). Closer to the sidewalls, since the impacting flow has lost its intensity the thermal boundary layer can also develop. It is interesting to note that the small recirculation vortices form very close to the two corners and that they associated with a localized region of hot fluid.

We now investigate the spatial evolution of the mean temperature on the heated convex wall (see figure 11). T is plotted in function of s/D_h in the symmetry plane at $z/D_h = 0.5$ and closer to the sidewalls at $z/D_h = 0.25$. We observe that T is higher at $Re = 12000$ than at $Re = 6000$ with a quasi constant difference close to 8 % between the two profiles throughout the duct width. From $s/D_h = 0.2D_h$ the temperature starts increasing with a faster increase in the high Reynolds number case. This is can be explained in the following way: the viscosity is reduced at high Reynolds number. Since the Prandtl number is taken equal to 0.7, the viscosity decrease induces a diminution of the fluid conductivity k. The fixed value of the heat flux necessarily imposes a larger temperature difference between the wall temperature and the fluid in the duct core. The incoming fluid temperature being identical for both cases, the wall temperature is consequently higher for the large Reynolds number value. Once the fluid enters the curved part, the temperature growth becomes linear with a growth rate which is similar for both values of the Reynolds

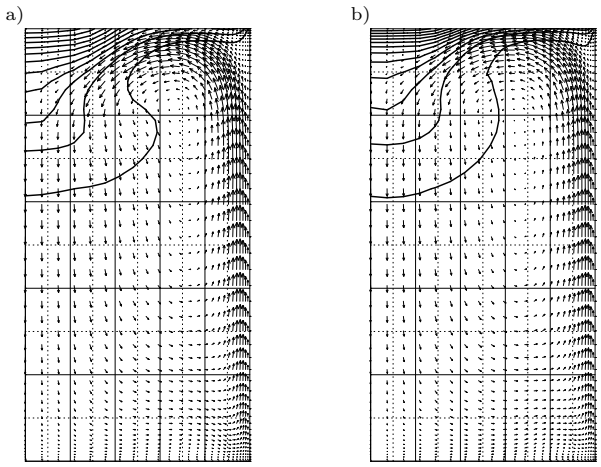

Figure 9: Half cross sections of the mean secondary flow and temperature isolines at the end of the curved part : a) $Re = 6000$, b) $Re = 12000$

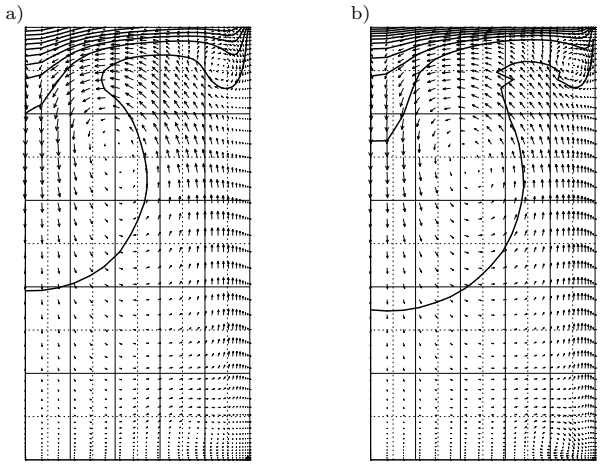

Figure 10: Half cross sections of the mean secondary flow and temperature isolines at the outflow : a) $Re = 6000$, b) $Re = 12000$

number. In both cases, the temperature growth extends further downstream in the symmetry plane $z/D_h = 0.5$ than in the intermediate plane $z/D_h = 0.25$. The establishment of the secondary cells indeed induces an early decrease of the temperature for $z/D_h = 0.25$ due to the cold fluid from the core impacting the heated wall. Conversely, the temperature keeps increasing in the duct central plane due to the stagnation of the hot fluid in that region. The temperature reaches maximum values as high as $T/T_w = 1.42$ at $Re = 12000$ and $T/T_w = 1.32$ at $Re = 6000$.

The temperature difference between the central plane and the intermediate plane is maximum at the end of the curved part where the Ekman vortices have reached their maximum intensity. The progressive attenuation of the intensity of these vortices after the curved part is associated with a temperature increase at the intermediate z location. As previously shown the increase in size of the vortices yields a more efficient ejection of the hot fluid from the central part of the heated wall towards the duct centre and a temperature decrease in that region.

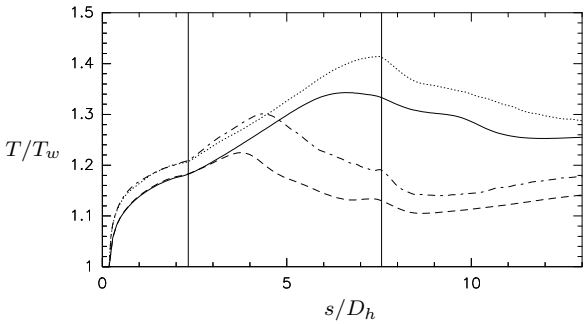

Figure 11: Profiles of T for $Re = 6000$ —— and – – – and for $Re = 12000$ ····· and —·— at $z/D_h = 0.5$ and $z/D_h = 0.25$ respectively

On figure 12, the profiles of the temperature T on the convex wall are plotted as a function of z/D_h at four downstream locations: at the beginning, the middle, the end of the curved part and at the outflow. It confirms that the global augmentation of temperature is more important at $Re = 12000$. At the beginning of the curved part, the profiles are quasi uniform showing that the development of the thermal boundary layer is identical whatever the distance from the duct corner. Because of the subsequent formation of the Ekman vortices, we assist to a significant temperature amplification for $z/D_h > 0.3$ and a diminution closer to the sidewalls due to the impinging cold fluid from the duct core. The transverse temperature gradient on the heated wall reaches its maximum at the end of the curved section and is more important at high Reynolds number. The progressive disappearance of the Ekman vortices in the straight exit part of the duct is associated with an attenuation of this gradient and the return to a more uniform temperature profile.

CONCLUSION

LES of the turbulent flow in curved heated ducts with square cross-section have been carried out with two different Reynolds number : $Re = 6000$ and $Re = 12000$. The aim is to investigate the influence of the Reynolds number on the flow and on the coherent structures. In the straight inlet part of the duct, the system of counter rotating cells is located closer to the duct corners when the Reynolds number increases. In the curved portion of the duct, a strong secondary transverse flow appears due to the radial pressure gradient between the two curved walls which eventually yields the formation of Ekman vortices. At the higher Reynolds, these become wider and their centre is moved away from the duct corner. We then study the heat transfers mechanisms within the duct by imposing a uniform heat flux on the convex wall. The Ekman vortices are found to be associated with a significant temperature gradient on the heated wall. These vortices induce an impingement of cold fluid from the duct core in the region of the heated wall located between the middle plane and the duct corner. This impinging flow gives rise to a converging transverse flow towards the duct middle plane and a stagnation region close to the heated wall where a significant temperature increase is observed. The Ekman vortices are therefore

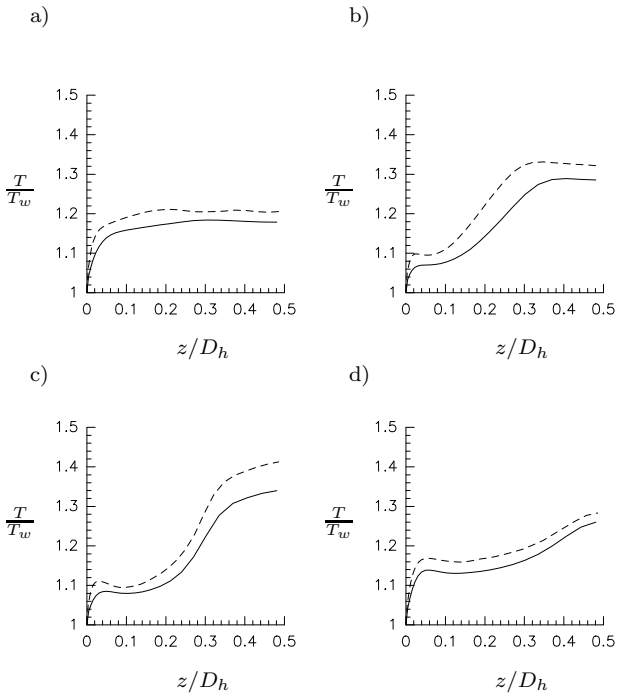

Figure 12: Profiles of T/T_w on the convex heated wall as a function of z/D_h for $Re = 6000$ —— and $Re = 12000$ – – – at a) the beginning of the curved part, b) the middle of the curved part, c) the end of curved part and d) at the outflow

associated with a significant transverse temperature gradient on the heated wall. This gradient is even more pronounced at high Reynolds number. In practical situations, this strong gradient can yield important transverse thermal constraints and the material alteration of the heated wall.

REFERENCES

Chang S.M., Humphrey J.A.C., and Modavi A., 1983, "Turbulent flow in a strongly curved U-bend and Downstream tangent of square cross-sections", *PhysicoChemical Hydrodynamics*, vol.4(3), pp. 243-269.

Gessner F.B., 1973, "The origin of secondary flow in turbulent flow along a corner.", *Journal of Fluid Mechanics*, vol.58, pp. 1-25.

Hébrard J., Métais O., and Salinas Vasquez M., 2004, "Large-eddy simulation of turbulent duct flow : heating and curvature effects", *International Journal of Heat and Fluid Flow*, vol.25, pp. 569-580.

Hoffman P.H., Muck K.C., and Bradshaw P., 1985, "The effect of concave surface curvature on turbulent boundary layers", *Journal of Fluid Mechanics*, vol.161, pp. 371-403.

Humphrey J.A.C., Whitelaw J.H., and Yee G., 1981, "Turbulent flow in square duct of strong curvature", *Journal of Fluid Mechanics*, vol.103, pp. 443-463.

Hunt I.A., and Joubert P.N., 1979, "Effects of small streamline curvature on turbulent duct flow", *Journal of Fluid Mechanics*, vol.91, part4, pp. 633-659.

Hunt J.R.C., Wray A.A., and Moin P., 1988, "Eddies, stream, and convergence zones in turbulent flows." Annual research briefs, Center for Turbulence Research, Stanford

Kennedy C.A., and Carpenter M.H., 1997, "Comparison of several numerical Methods for simulation of compressible shear layers", NASA technical paper, 3484.

Moser R.D., and Moin P., 1987, "The effects of curvature in wall-bounded turbulent flows", *Journal of Fluid Mechanics*, vol.175, pp. 479-510.

Muck K.C., Hoffman P.H., and Bradshaw P., 1985, "The effect of convex surface curvature on turbulent boundary layers", *Journal of Fluid Mechanics*, vol.161, pp. 347-369.

Münch C., Hébrard J., and Métais O., 2004, "Large eddy simulation of turbulent flow in curved and S-shape ducts.", *Direct and Large Eddy Simulation V*, pp. 527-536.

Poinsot T., and Lele S., 1992, "Boundary conditions for direct simulations of compressible viscous flows.", *Journal of Computational Physics.*, vol. 101, pp. 104-129.

Salinas M., and Métais O., 2002, "Large eddy simulation of spatially growing thermal boundary layer in a turbulent square duct.", *Direct and Large eddy simulation IV*, pp. 277-284.

Silva Lopes A., and Piomelli U., 2003, "Large eddy simulation of the flow in an S-duct", AIAA 0964, pp. 1-14.